Optomagnetism with a plasmonic skyrmion

VAGE KARAKHANYAN[1] AND THIERRY GROSJEAN[1,*]

[1] Optics Department – FEMTO-ST Institute UMR 6174 - University of Franche-Comté – CNRS - Besançon, France
[*] Corresponding author: thierry.grosjean@univ-fcomte.fr

Compiled November 15, 2024

Research at the frontier between optics and magnetism is revealing a wealth of innovative phenomena and avenues of exploration. Optical waves are demonstrating the capacity to induce ultrafast magnetism, while optical analogs of magnetic states, such as magnetic skyrmions, offer the prospect of novel spin-optical states. In this paper, we strengthen the synergy between light and magnetism by exploring the ability of plasmonic Neel skyrmions to create an optomagnetic field, i.e., an opto-induced stationary magnetic field, within a thin gold film. We show that, when generated using a focused radially-polarized vortex beam, a plasmonic Neel skyrmion emerges as an optimum for inducing optomagnetism in a thin gold film. Optical skyrmions offer new degrees of freedom for enhancing and controlling optomagnetism in plasmonic nanostructures, with direct application in all-optical magnetization switching, magnetic recording, and the excitation of spin waves.

http://dx.doi.org/10.1364/ao.XX.XXXXXX

Magnetic skyrmions are topologically-protected magnetic states showing space-variant spin distributions [1]. Since their first observation in 2009 [2–4] these spin textures have attracted much interest from both fundamental aspects and potential applications in novel spintronic devices.

Recently, the concept of magnetic skyrmion has been extended to optics, leading to novel optical-field or optical-spin textures on the subwavelength scale [5, 6]. As their magnetic counterpart, optical skyrmions of different structures can be densely packed in square or hexagonal lattices [5, 7]. Optical skyrmions are a promising building block of the emerging spin-based optics, including optical nano-imaging, quantum information processing, metrology and data storage.

In this paper, we study the ability of a Neel-type optical skyrmion to generate an optomagnetic field via the inverse Faraday effect (IFE) [8–10]. The IFE has been extensively explored due to its potential to generate ultrafast magnetic data storage [11–13] and non-contact excitation of spin-waves [14–18]. Moreover, the IFE can be enhanced and tailored via the excitation of surface plasmons in noble metals [19–28] and in hybrid structures combining noble metals and magnetic materials [29–32]. Since the IFE is induced by both the SAM and OAM of light, spin-orbit interaction plays a significant role in the optomagnetism [33]. The spin texture of an optical Neel skyrmion, which is also strongly influenced by spin-orbit interaction [5, 6, 34], presents new avenues for generating and controlling optomagnetism. We show here that plasmonic Neel Skyrmion holds promise to maximize optomagnetic effects in a thin gold film. The optical counterpart of magnetic skyrmions offers intriguing solutions to increase and control optomagnetic effects is nanostructures.

A plasmonic Neel skyrmion is a metal/air surface mode whose electric field or spin angular momentum (SAM) density is topologically invariant and radially distributed along the surface. Following the approaches introduced by Du et al. [6] and Tsesses et al. [5], we investigate plasmonic Neel skyrmions by tightly focusing either a radially-polarized vortex beam (RPVB) of topological charge $l = \pm 1$ or a circularly polarized beam (CPB) onto a thin gold film lying on a glass substrate (Fig. 1(a)). In the following, the plasmonic Neel skyrmions obtained with the RPVB and CPB will be referred to as Skyrmion-R and Skyrmion-C, respectively.

RPVB belong to the family of the vector vortex beams, characterized by an inhomogeneous vector polarization state and a helical phase [35–37]. The waist of the incoming RVPB and CPB, characterized by a Gaussian profile, is projected onto the exit pupil plane of a microscope objective where it is spatially filtered with an narrow annular slit within an opaque screen. The annular pupil restricts the incidence angles of incoming light waves to a narrow range around a mean value defined by the slit diameter. This angular range is set either at 1° or 0.1°, regardless of the average incidence angle. The $1/e$ width of the beam waist coincides with the pupil diameter of the microscope objective, whose numerical aperture (NA) of 1.3 enables light focusing in the substrate beyond the critical angle.

Using the theory established by Richards and Wolf [38, 39], the electric optical field at focus reads:

$$\mathbf{E}(r,\xi,z) = -\frac{ik_1 f \exp[-ik_1 f]}{2\pi}\frac{1}{\sqrt{n_1}}\times \int_{\theta_0-\frac{\Delta\theta}{2}}^{\theta_0+\frac{\Delta\theta}{2}} G(\theta)\int_0^{2\pi}\mathbf{e}(\theta,\psi,z)\exp\left[i\alpha r\cos(\psi-\xi)\right]d\theta d\psi, \quad (1)$$

where $G(\theta) = \cos^{\frac{1}{2}}(\theta)\sin(\theta)F(\theta)$, (r,ξ,z) are cylindrical coordinates, f is the focal length of the microscope objective, θ and ψ are directional angles and α is a function of θ. $\Delta\theta$ is the focusing angular range. $k_1 = 2\pi n_1/\lambda$, where λ is the wavelength and n_1 is the refractive index of the substrate.

For the RPVB of the first order leading to the Skyrmion-R,

the vector $\mathbf{e}(\theta,\psi,z)$ takes the form:

$$\mathbf{e}(\theta,\psi,z) = \mathbf{e_{TM}}(\theta,\psi,z) \propto \exp[\pm i\psi]\begin{pmatrix} -t^r_{TM}(z)\cos\theta\cos\psi \\ -t^r_{TM}(z)\cos\theta\sin\psi \\ t^z_{TM}(z)\sin\theta \end{pmatrix} \quad (2)$$

t^r_{TM} and t^z_{TM} are coefficients under the form $C^+_{TM}\exp[iw_2z] + C^-_{TM}\exp[-iw_2z]$ where w_2 is the component of the wave vector normal to the surfaces and $i=\sqrt{-1}$. Coefficients C^+_{TM} and C^-_{TM} are obtained by applying boundary conditions of the optical fields at the metal surfaces (see for instance in Ref. [40]).

For a CPB leading to the Skyrmion-C, the vector $\mathbf{e}(\theta,\psi,z)$ is written as:

$$\mathbf{e}(\theta,\psi,z) \propto -\frac{\sqrt{2}}{2}\left[\mathbf{e_{TM}}(\theta,\psi,z) + i\mathbf{e_{TE}}(\theta,\psi,z)\right], \quad (3)$$

where,

$$\mathbf{e_{TE}}(\theta,\psi,z) = t_{TE}(z)\exp[\pm i\psi]\begin{pmatrix} -\sin\psi \\ \cos\psi \\ 0 \end{pmatrix}. \quad (4)$$

t_{TE} is a coefficient under the form $C^+_{TE}\exp[iw_2z] + C^-_{TE}\exp[-iw_2z]$. Coefficients C^+_{TE} and C^-_{TE} are obtained by applying boundary conditions of the optical fields at the metal surfaces. The phase term $exp[\pm i\psi]$ in Eq. 4 reveals spin-orbit interaction at focus [41].

The apodization function at the pupil plane of the microscope objective is approximated by the function:

$$F(\theta) = \frac{2}{w_0}\sqrt{\frac{Z_0P_0}{\pi}}\exp\left[\frac{-f^2\sin^2\theta}{w_0^2}\right], \quad (5)$$

with $w_0 = f\sin\theta_M$.

P_0 and w_0 are the power and $1/e$ width of the incoming paraxial beam and Z_0 is the vacuum impedance. The optical magnetic field is calculated by replacing $\mathbf{e}(r,\xi,z)$ by $\mathbf{h}(r,\xi,z) = \mathbf{k}\times\mathbf{e}(r,\xi,z)/\omega\mu_0$ in Eq. 1. ω and μ_0 are the angular frequency and permeability of vacuum, respectively.

At focus, the SAM density of the fields transmitted through the gold film is defined as:

$$\mathbf{s} = \left[\mathrm{Im}(\varepsilon_0\mathbf{E}\times\mathbf{E}^*) + \mathrm{Im}(\mu_0\mathbf{H}\times\mathbf{H}^*)\right]/2\omega, \quad (6)$$

where ε_0 is the permittivity of vacuum [42, 43]. The SAM density can also be expressed as:

$$\mathbf{s} = \frac{w}{\omega}\sigma, \quad (7)$$

where $w = 1/2\left[\varepsilon_0|\mathbf{E}|^2 + \mu_0|\mathbf{H}|^2\right]$ is the energy density and σ is the local polarization helicity vector. The three components of σ are comprised between -1 and 1, the values 0 and ±1 correspond to the linear and circular polarization states, respectively.

To confirm the analogy to magnetic skyrmions, we calculate the skyrmion number (n) associated with the SAM distribution:

$$n = \frac{1}{4\pi}\int_A \mathbf{S_n}\cdot\left(\frac{\partial\mathbf{S_n}}{\partial x}\times\frac{\partial\mathbf{S_n}}{\partial y}\right)dxdy, \quad (8)$$

where S_n is the unit vector in the direction of the local SAM, A is the area of the unit cell of the skyrmion. When $n=1$, the photonic spin structure is the analogue to the magnetization texture of either a Neel or a Bloch skyrmion in magnetic materials [44, 45]. An analysis of the vector spin distribution allows to identify the exact nature of the optical skyrmion.

On the basis of a hydrodynamic model of free electrons in metals, we have recently proposed a new framework to describe the IFE in plasmonic nanostructures [27, 28, 33]. In the present study, the opto-induced drift current densities within the metal film are represented as follows:

$$J^b_\xi \approx \frac{2\mu_0|\gamma_\omega|^2}{n_0e}\langle\mathbf{\Pi}\rangle_\xi, \quad (9)$$

in the metal bulk, and:

$$J^s_\xi \approx \pm\frac{|\gamma_\omega|^2}{n_0e\omega}\,\mathrm{Im}\left[E^z_\omega(0^-)E^{\xi*}_\omega(0^-)\right], \quad (10)$$

at the two metal surfaces [27, 33]. $\langle\mathbf{\Pi}\rangle_\xi$ is the azimuthal component of the time averaged Poynting vector $\langle\mathbf{\Pi}\rangle = 0.5\,\mathrm{Re}\,(\mathbf{E}\times\mathbf{H}^*)$. $E^z_\omega(0^-)$ and $E^\xi_\omega(0^-)$ are the longitudinal and azimuthal components of the optical electric field at the two metal surfaces. The $+$ and $-$ signs in Eq. 10 correspond to the current densities at the lower and upper interfaces of the metal film, respectively. The optomagnetic field is deduced from Eqs. 9 and 10 by using the Biot and Savart law:

$$\mathbf{B}(\mathbf{r}) = \frac{\mu_0}{4\pi}\iiint_V\frac{J_d(\mathbf{r}')\wedge(\mathbf{r}-\mathbf{r}')}{|\mathbf{r}-\mathbf{r}'|^3}\,d^3r', \quad (11)$$

where $\mathbf{r}$ and $\mathbf{r}'$ are space coordinate vectors and the drift current density $J_d = J^s_\xi + J^b_\xi$ groups bulk and surface contributions.

The calculations are performed at a wavelength of $\lambda = 800$ nm. We identify a surface plasmon excitation at an incidence angle θ of 43.25° (following the Kretschmann configuration; see Fig. 1(b)). Figure 1(b) shows that optical skyrmions occur beyond the critical angle of 41.8° for both incoming polarizations. The radially-distributed spin texture observed at plasmon resonance for the Skyrmion-R is that of a Neel skyrmion (Figs. 1(c)). A similar spin texture is observed for the Skyrmion-C. Outside the plasmon resonance, below the critical angle, the SAM texture transitions to an azimuthally polarized state, akin to the magnetization texture observed in Bloch skyrmions. The skyrmion number is however insufficient to categorize the optical field as an optical analogue to the Bloch skyrmion.

Fig. 2 shows the optomagnetic response of the thin gold film under illumination with $\Delta\theta = 1°$. Upon scanning the average incidence angle, the total optomagnetic energy (defined in the inset of Fig. 2(a)) peaks right at the plasmon angle ($\theta_0 = 42.95°$) for both incident polarization states (Fig. 2(a)). At surface plasmon excitation, the optomagnetic energy is enhanced by approximately 13-fold and 128-fold for the Skyrmion-R and Skyrmion-C, respectively. This confirms the role of surface plasmons in amplifying optomagnetism in metals. However, the Skyrmion-R and Skyrmion-C result in distinct levels of optomagnetism: the optomagnetic energy is 11.5 times larger with the Skyrmion-R.

Figs. 2(b) and (c) show the optomagnetic field generated by the Skyrmion-R and Skyrmion-C, respectively. With the Skyrmion-R (Fig. 2(b)), the maximum optomagnetic field is localized at the upper surface of the gold film. Off-resonance, at $\theta_0 = 37°$ (Fig. 2(d)), the optomagnetic field is confined at the lower interface with its maximum reduced by a factor of 3. In

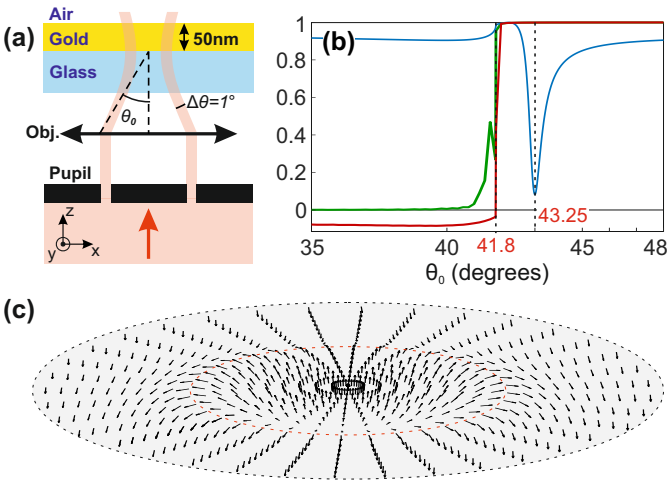

Fig. 1. (a) Schematic diagram of the focusing system designed to generate Neel-type plasmonic skyrmions. (b) Blue line: reflectance of the thin gold film as a function of the incidence angle of a TM-polarized plane wave in the glass substrate (λ=800 nm). Red and green lines: skyrmion number of the field transmitted through the thin gold film versus the mean incidence angle of the focused beam, for the RPVB and the CPB, respectively. The skyrmion number is calculated at a distance of 10 nm beyond the top surface. Focusing occurs across an angular range $\Delta\theta = 0.1°$. The pair of vertical dashed lines identify the critical angle of total internal reflection and the plasmon resonance angle, which are equal to 41.8° and 43.25°, respectively. (c) Distribution of the SAM orientation for the Skyrmion-R within its unit cell, calculated at 10 nm above the top surface of the gold layer at $\theta_0 = 43.25°$. The arrows indicate the direction of the unit SAM vector.

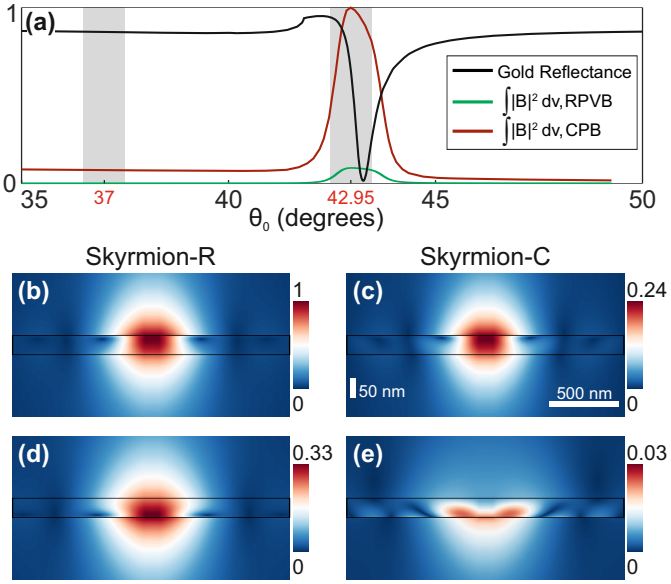

Fig. 2. (a) Blue curve: Reflectance of the metal film versus the incidence angle of a TM-polarized plane wave in the glass substrate (λ=800 nm). Red and green curves: total energy of the optomagnetic field induced by a focused RPVB (cf. Skyrmion-R) and a CPB (Skyrmion-C), respectively, versus the focusing angle θ_0. (b,c) Amplitude of the optomagnetic field in a longitudinal cross-section, for (b) the Skyrmion-R, and (c) the Skyrmion-C.(d) and (e) Amplitude of the optomagnetic field calculated under the same conditions as (b) and (c), respectively, but off-resonance (at $\theta_0 = 37°$). $\Delta\theta = 1°$ falls within the shaded regions depicted in (a).

comparison, with incoming circular polarization, the optomagnetic field is attenuated by a factor of 4 with the Skyrmion-C (Fig. 2(c)) and by a factor of 30 outside the plasmon resonance (Fig. 2(e)).

The optomagnetic fields obtained with the Skyrmion-R and Skyrmion-C show similar spatial distributions (Figs. 2(b) and (c)). A similar morphology of the optomagnetic field is maintained off the resonance of the Skyrmion-R (cf. Figs. 2(b) and (d)), but it is lost outside the resonance of the Skyrmion-C (cf. Figs. 2(c) and (e)).

As plasmonic eigenmodes, the Skyrmion-R and Skyrmion-C are bound to an axis-symmetrical "TM optical state" within the metal film, composed of TM-polarized Fourier components (surface plasmons are TM-polarized optical waves [39]). The expressions of these Fourier components are defined in Eq. 2.

In the case of an incoming RPVB, the entirety of the incident field intensity contributes to the generation of the TM optical state within the metal film, i.e., to the Skyrmion-R at plasmon resonance (cf. Eq 2). By comparing Eqs. 2 and 3, we see that only half of the incident field intensity is involved in the generation of a Skyrmion-C. In the case of an incoming CPB, the TM optical state associated with the Skyrmion-C in the metal film is combined to an axis-symmetrical "TE optical state" (see Eqs. 1, 3 and 4). The "TE optical state", constituted of TE-polarized Fourier components, is primarily confined within the skin depth at the lower interface.

As the surface and volume current densities stem from a second-order nonlinear optical effect (see Eqs. 9 and 10) [27], the Skyrmion-R exhibits twice the efficiency in generating opto-induced drift currents compared to the Skyrmion-C, as shown in Fig. 3. Since the TE optical state is confined within the lower skin depth, the drift current densities induced with the Skyrmion-R and Skyrmion-C exhibit similar spatial distributions in the upper half of the gold film, as shown in Figs. 3(a,b) and 3(e,f). However, the Skyrmion-C results in a maximum amplitude of the drift current densities that is halved.

The Skyrmion-R generates surface and volume drift current densities with the same handedness, forming a uniform current loop (see Figs. 3(a,c,e)). In contrast, the presence of a TE optical state with the Skyrmion-C induces a pair of current loops with opposite handedness in the lower half of the metal film, which is less efficient in generating an optomagnetic field (Figs. 3(d,f)). Therefore, the existence of TE optical states in the plasmonic film both attenuates amplitude of the Skyrmion-C compared to the Skyrmion-R and hinders the optomagnetic effect in the lower half of the metal film. As a result, the optomagnetic field is reduced by four with the Skyrmion-C compared to the Skyrmion-R (which lacks TE optical state). Therefore, being generated from a pure TM optical state within a thin gold film, Skyrmion-R emerges as an optimum for generating plasmon-induced magnetism.

To conclude, an optical counterpart of magnetic Neel skyrmion is shown to generate a static magnetic field in a thin gold film, via plasmon-enhanced IFE. Plasmonic Neel skyrmions produced by focusing a RPVB (cf. Skyrmion-R) [6] are shown to be optimal for generating optomagnetism in a thin gold film. More generally, vector vortex beams appear as a promising al-

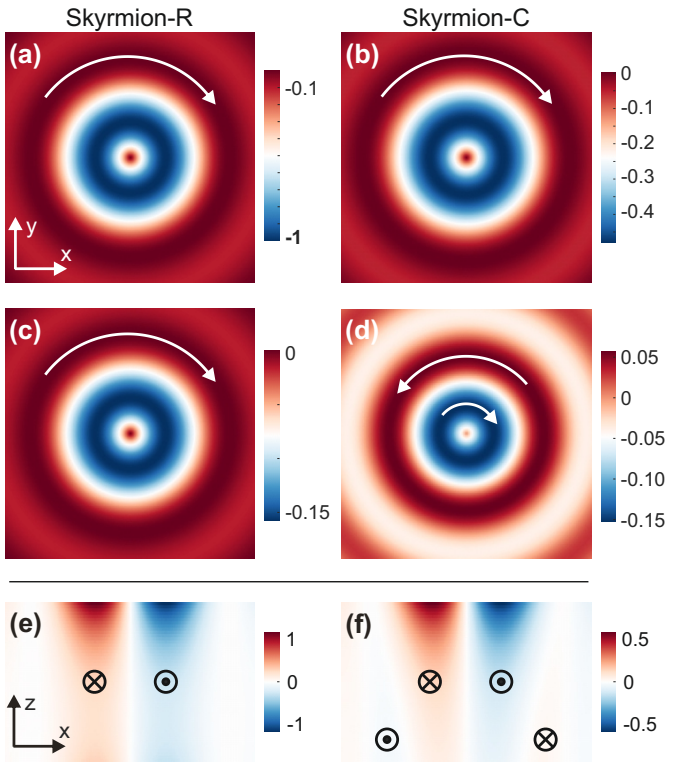

Fig. 3. (a-d) Normalized current densities at (a,b) the upper and (c,d) lower surfaces of the thin gold film, with (a,c) a Skyrmion-R and (b,d) a Skyrmion-C. (e,f) Normalized volume current densities in a (xz) cross-section perpendicular to the surfaces, with the Skyrmion-R and Skyrmion-C, respectively.

ternative to CPB for creating and controlling plasmon-induced magnetism in metal films, and by extension, in resonant plasmonic nanoantennas.

FUNDING

EIPHI Graduate School (contract ANR-17-EURE-0002); Region "Bourgogne Franche-Comte"; French Agency of Research (contracts ANR-18-CE42-0016 and ANR-23-CE42-0021); French Renatech network; Equipex+ Nanofutur (21-ESRE-0012)

DISCLOSURES

The authors declare no conflicts of interest.

REFERENCES

1. A. Fert, V. Cros, and J. Sampaio, Nat. nanotechnology **8**, 152 (2013).
2. S. Muhlbauer, B. Binz, F. Jonietz, C. Pfleiderer, A. Rosch, A. Neubauer, R. Georgii, and P. Boni, Science **323**, 915 (2009).
3. A. Neubauer, C. Pfleiderer, B. Binz, A. Rosch, R. Ritz, P. Niklowitz, and P. Böni, Phys. review letters **102**, 186602 (2009).
4. C. Pappas, E. Lelievre-Berna, P. Falus, P. Bentley, E. Moskvin, S. Grigoriev, P. Fouquet, and B. Farago, Phys. review letters **102**, 197202 (2009).
5. S. Tsesses, E. Ostrovsky, K. Cohen, B. Gjonaj, N. Lindner, and G. Bartal, Science **361**, 993 (2018).
6. L. Du, A. Yang, A. V. Zayats, and X. Yuan, Nat. Phys. **15**, 650 (2019).
7. X. Lei, A. Yang, P. Shi, Z. Xie, L. Du, A. V. Zayats, and X. Yuan, Phys. Rev. Lett. **127**, 237403 (2021).
8. P. Pershan, J. Van der Ziel, and L. Malmstrom, Phys. review **143**, 574 (1966).
9. D. Popova, A. Bringer, and S. Blügel, Phys. Rev. B **84**, 214421 (2011).
10. R. Hertel, J. Magn. Magn. Mater. **303**, L1 (2006).
11. E. Beaurepaire, J.-C. Merle, A. Daunois, and J.-Y. Bigot, Phys. Rev. Lett. **76**, 4250 (1996).
12. C. Stanciu, F. Hansteen, A. Kimel, A. Kirilyuk, A. Tsukamoto, A. Itoh, and T. Rasing, Phys. Rev. Lett. **99**, 047601 (2007).
13. A. Kirilyuk, A. V. Kimel, and T. Rasing, Rev. Mod. Phys. **82**, 2731 (2010).
14. A. Kimel, A. Kirilyuk, P. Usachev, R. Pisarev, A. Balbashov, and T. Rasing, Nature **435**, 655 (2005).
15. A. Kalashnikova, A. Kimel, R. Pisarev, V. Gridnev, P. Usachev, A. Kirilyuk, and T. Rasing, Phys. Rev. B **78**, 104301 (2008).
16. T. Satoh, Y. Terui, R. Moriya, B. A. Ivanov, K. Ando, E. Saitoh, T. Shimura, and K. Kuroda, Nat. Photonics **6**, 662 (2012).
17. I. Savochkin, M. Jäckl, V. Belotelov, I. Akimov, M. Kozhaev, D. Sylgacheva, A. Chernov, A. Shaposhnikov, A. Prokopov, V. Berzhansky *et al.*, Sci. Rep. **7**, 1 (2017).
18. K. Matsumoto, I. Yoshimine, K. Himeno, T. Shimura, and T. Satoh, Phys. Rev. B **101**, 184407 (2020).
19. I. I. Smolyaninov, C. C. Davis, V. N. Smolyaninova, D. Schaefer, J. Elliott, and A. V. Zayats, Phys. Rev. B **71**, 035425 (2005).
20. Y. Gu and K. G. Kornev, JOSA B **27**, 2165 (2010).
21. O. H.-C. Cheng, D. H. Son, and M. Sheldon, Nat. Photon. **14**, 365 (2020).
22. K. Koshelev, V. Y. Kachorovskii, and M. Titov, Phys. Rev. B **92**, 235426 (2015).
23. S. Hamidi, M. Razavinia, and M. Tehranchi, Opt. Commun. **338**, 240 (2015).
24. A. Nadarajah and M. T. Sheldon, Opt. Express **25**, 12753 (2017).
25. J. Hurst, P. M. Oppeneer, G. Manfredi, and P.-A. Hervieux, Phys. Rev. B **98**, 134439 (2018).
26. R. Mondal, M. Berritta, C. Paillard, S. Singh, B. Dkhil, P. M. Oppeneer, and L. Bellaiche, Phys. Rev. B **92**, 100402 (2015).
27. V. Karakhanyan, Y. Lefier, C. Eustache, and T. Grosjean, Opt. Lett. **46**, 613 (2021).
28. V. Karakhanyan, C. Eustache, Y. Lefier, and T. Grosjean, OSA Continuum **4**, 1598 (2021).
29. A. H. Chu, B. Beauchamp, D. Shah, A. Boltasseva, V. M. Shalaev, E. E. Marinero *et al.*, Opt. Mat. Express **10**, 3107 (2020).
30. D. Ignatyeva, C. Davies, D. Sylgacheva, A. Tsukamoto, H. Yoshikawa, P. Kapralov, A. Kirilyuk, V. Belotelov, and A. Kimel, Nat. Commun. **10**, 1 (2019).
31. S.-J. Im, J.-S. Pae, C.-S. Ri, K.-S. Ho, and J. Herrmann, Phys. Rev. B **99**, 041401 (2019).
32. F. Cheng, C. Wang, Z. Su, X. Wang, Z. Cai, N. X. Sun, and Y. Liu, Nano Lett. **20**, 6437 (2020).
33. V. Karakhanyan, C. Eustache, Y. Lefier, and T. Grosjean, Phys. Rev. B **105**, 045406 (2022).
34. P. Shi, L. Du, C. Li, A. V. Zayats, and X. Yuan, Proc. Nat. Aca. Sci. **118**, e2018816118 (2021).
35. X. Hao, C. Kuang, T. Wang, and X. Liu, Opt. letters **35**, 3928 (2010).
36. Z. Zhao, J. Wang, S. Li, and A. E. Willner, Opt. letters **38**, 932 (2013).
37. C.-W. Qiu, D. Palima, A. Novitsky, D. Gao, W. Ding, S. V. Zhukovsky, and J. Gluckstad, Nanophotonics **3**, 181 (2014).
38. B. Richards and E. Wolf, Proc. Royal Soc. London. Ser. A. Math. Phys. Sci. **253**, 358 (1959).
39. L. Novotny and B. Hecht, *Principles of nano-optics* (Cambridge university press, 2012).
40. M. Born and E. Wolf, *Principles of optics: electromagnetic theory of propagation, interference and diffraction of light* (Elsevier, 2013).
41. K. Y. Bliokh, D. Smirnova, and F. Nori, Science **348**, 1448 (2015).
42. M. V. Berry, J.Opt. A **11**, 094001 (2009).
43. K. Y. Bliokh, A. Y. Bekshaev, and F. Nori, Nat. Commun. **5**, 3300 (2014).
44. S. Bera and S. S. Mandal, Phys. Rev. Res. **1**, 033109 (2019).
45. X. Yu, W. Koshibae, Y. Tokunaga, K. Shibata, Y. Taguchi, N. Nagaosa, and Y. Tokura, Nature **564**, 95 (2018).

FULL REFERENCES

1. A. Fert, V. Cros, and J. Sampaio, "Skyrmions on the track," Nat. nanotechnology **8**, 152–156 (2013).
2. S. Muhlbauer, B. Binz, F. Jonietz, C. Pfleiderer, A. Rosch, A. Neubauer, R. Georgii, and P. Boni, "Skyrmion lattice in a chiral magnet," Science **323**, 915–919 (2009).
3. A. Neubauer, C. Pfleiderer, B. Binz, A. Rosch, R. Ritz, P. Niklowitz, and P. Böni, "Topological hall effect in the a phase of mnsi," Phys. review letters **102**, 186602 (2009).
4. C. Pappas, E. Lelievre-Berna, P. Falus, P. Bentley, E. Moskvin, S. Grigoriev, P. Fouquet, and B. Farago, "Chiral paramagnetic skyrmion-like phase in mnsi," Phys. review letters **102**, 197202 (2009).
5. S. Tsesses, E. Ostrovsky, K. Cohen, B. Gjonaj, N. Lindner, and G. Bartal, "Optical skyrmion lattice in evanescent electromagnetic fields," Science **361**, 993–996 (2018).
6. L. Du, A. Yang, A. V. Zayats, and X. Yuan, "Deep-subwavelength features of photonic skyrmions in a confined electromagnetic field with orbital angular momentum," Nat. Phys. **15**, 650–654 (2019).
7. X. Lei, A. Yang, P. Shi, Z. Xie, L. Du, A. V. Zayats, and X. Yuan, "Photonic spin lattices: symmetry constraints for skyrmion and meron topologies," Phys. Rev. Lett. **127**, 237403 (2021).
8. P. Pershan, J. Van der Ziel, and L. Malmstrom, "Theoretical discussion of the inverse faraday effect, raman scattering, and related phenomena," Phys. review **143**, 574 (1966).
9. D. Popova, A. Bringer, and S. Blügel, "Theory of the inverse faraday effect in view of ultrafast magnetization experiments," Phys. Rev. B **84**, 214421 (2011).
10. R. Hertel, "Theory of the inverse faraday effect in metals," J. Magn. Magn. Mater. **303**, L1–L4 (2006).
11. E. Beaurepaire, J.-C. Merle, A. Daunois, and J.-Y. Bigot, "Ultrafast spin dynamics in ferromagnetic nickel," Phys. Rev. Lett. **76**, 4250 (1996).
12. C. Stanciu, F. Hansteen, A. Kimel, A. Kirilyuk, A. Tsukamoto, A. Itoh, and T. Rasing, "All-optical magnetic recording with circularly polarized light," Phys. Rev. Lett. **99**, 047601 (2007).
13. A. Kirilyuk, A. V. Kimel, and T. Rasing, "Ultrafast optical manipulation of magnetic order," Rev. Mod. Phys. **82**, 2731 (2010).
14. A. Kimel, A. Kirilyuk, P. Usachev, R. Pisarev, A. Balbashov, and T. Rasing, "Ultrafast non-thermal control of magnetization by instantaneous photomagnetic pulses," Nature **435**, 655–657 (2005).
15. A. Kalashnikova, A. Kimel, R. Pisarev, V. Gridnev, P. Usachev, A. Kirilyuk, and T. Rasing, "Impulsive excitation of coherent magnons and phonons by subpicosecond laser pulses in the weak ferromagnet febo 3," Phys. Rev. B **78**, 104301 (2008).
16. T. Satoh, Y. Terui, R. Moriya, B. A. Ivanov, K. Ando, E. Saitoh, T. Shimura, and K. Kuroda, "Directional control of spin-wave emission by spatially shaped light," Nat. Photonics **6**, 662–666 (2012).
17. I. Savochkin, M. Jäckl, V. Belotelov, I. Akimov, M. Kozhaev, D. Sylgacheva, A. Chernov, A. Shaposhnikov, A. Prokopov, V. Berzhansky *et al.*, "Generation of spin waves by a train of fs-laser pulses: a novel approach for tuning magnon wavelength," Sci. Rep. **7**, 1–10 (2017).
18. K. Matsumoto, I. Yoshimine, K. Himeno, T. Shimura, and T. Satoh, "Observation of evanescent spin waves in the magnetic dipole regime," Phys. Rev. B **101**, 184407 (2020).
19. I. I. Smolyaninov, C. C. Davis, V. N. Smolyaninova, D. Schaefer, J. Elliott, and A. V. Zayats, "Plasmon-induced magnetization of metallic nanostructures," Phys. Rev. B **71**, 035425 (2005).
20. Y. Gu and K. G. Kornev, "Plasmon enhanced direct and inverse faraday effects in non-magnetic nanocomposites," JOSA B **27**, 2165–2173 (2010).
21. O. H.-C. Cheng, D. H. Son, and M. Sheldon, "Light-induced magnetism in plasmonic gold nanoparticles," Nat. Photon. **14**, 365–368 (2020).
22. K. Koshelev, V. Y. Kachorovskii, and M. Titov, "Resonant inverse faraday effect in nanorings," Phys. Rev. B **92**, 235426 (2015).
23. S. Hamidi, M. Razavinia, and M. Tehranchi, "Enhanced optically induced magnetization due to inverse faraday effect in plasmonic nanostructures," Opt. Commun. **338**, 240–245 (2015).
24. A. Nadarajah and M. T. Sheldon, "Optoelectronic phenomena in gold metal nanostructures due to the inverse faraday effect," Opt. Express **25**, 12753–12764 (2017).
25. J. Hurst, P. M. Oppeneer, G. Manfredi, and P.-A. Hervieux, "Magnetic moment generation in small gold nanoparticles via the plasmonic inverse faraday effect," Phys. Rev. B **98**, 134439 (2018).
26. R. Mondal, M. Berritta, C. Paillard, S. Singh, B. Dkhil, P. M. Oppeneer, and L. Bellaiche, "Relativistic interaction hamiltonian coupling the angular momentum of light and the electron spin," Phys. Rev. B **92**, 100402 (2015).
27. V. Karakhanyan, Y. Lefier, C. Eustache, and T. Grosjean, "Optomagnets in nonmagnetic plasmonic nanostructures," Opt. Lett. **46**, 613–616 (2021).
28. V. Karakhanyan, C. Eustache, Y. Lefier, and T. Grosjean, "Plasmon-induced 0.13 t optomagnetic field in a gold coaxial nanoaperture," OSA Continuum **4**, 1598–1608 (2021).
29. A. H. Chu, B. Beauchamp, D. Shah, A. Boltasseva, V. M. Shalaev, E. E. Marinero *et al.*, "Hybrid magneto photonic material structure for plasmon assisted magnetic switching," Opt. Mat. Express **10**, 3107–3118 (2020).
30. D. Ignatyeva, C. Davies, D. Sylgacheva, A. Tsukamoto, H. Yoshikawa, P. Kapralov, A. Kirilyuk, V. Belotelov, and A. Kimel, "Plasmonic layer-selective all-optical switching of magnetization with nanometer resolution," Nat. Commun. **10**, 1–7 (2019).
31. S.-J. Im, J.-S. Pae, C.-S. Ri, K.-S. Ho, and J. Herrmann, "All-optical magnetization switching by counterpropagataion or two-frequency pulses using the plasmon-induced inverse faraday effect in magnetoplasmonic structures," Phys. Rev. B **99**, 041401 (2019).
32. F. Cheng, C. Wang, Z. Su, X. Wang, Z. Cai, N. X. Sun, and Y. Liu, "All-optical manipulation of magnetization in ferromagnetic thin films enhanced by plasmonic resonances," Nano Lett. **20**, 6437–6443 (2020).
33. V. Karakhanyan, C. Eustache, Y. Lefier, and T. Grosjean, "Inverse faraday effect from the orbital angular momentum of light," Phys. Rev. B **105**, 045406 (2022).
34. P. Shi, L. Du, C. Li, A. V. Zayats, and X. Yuan, "Transverse spin dynamics in structured electromagnetic guided waves," Proc. Nat. Aca. Sci. **118**, e2018816118 (2021).
35. X. Hao, C. Kuang, T. Wang, and X. Liu, "Phase encoding for sharper focus of the azimuthally polarized beam," Opt. letters **35**, 3928–3930 (2010).
36. Z. Zhao, J. Wang, S. Li, and A. E. Willner, "Metamaterials-based broadband generation of orbital angular momentum carrying vector beams," Opt. letters **38**, 932–934 (2013).
37. C.-W. Qiu, D. Palima, A. Novitsky, D. Gao, W. Ding, S. V. Zhukovsky, and J. Gluckstad, "Engineering light-matter interaction for emerging optical manipulation applications," Nanophotonics **3**, 181–201 (2014).
38. B. Richards and E. Wolf, "Electromagnetic diffraction in optical systems, ii. structure of the image field in an aplanatic system," Proc. Royal Soc. London. Ser. A. Math. Phys. Sci. **253**, 358–379 (1959).
39. L. Novotny and B. Hecht, *Principles of nano-optics* (Cambridge university press, 2012).
40. M. Born and E. Wolf, *Principles of optics: electromagnetic theory of propagation, interference and diffraction of light* (Elsevier, 2013).
41. K. Y. Bliokh, D. Smirnova, and F. Nori, "Quantum spin hall effect of light," Science **348**, 1448–1451 (2015).
42. M. V. Berry, "Optical currents," J.Opt. A **11**, 094001 (2009).
43. K. Y. Bliokh, A. Y. Bekshaev, and F. Nori, "Extraordinary momentum and spin in evanescent waves," Nat. Commun. **5**, 3300 (2014).
44. S. Bera and S. S. Mandal, "Theory of the skyrmion, meron, antiskyrmion, and antimeron in chiral magnets," Phys. Rev. Res. **1**, 033109 (2019).
45. X. Yu, W. Koshibae, Y. Tokunaga, K. Shibata, Y. Taguchi, N. Nagaosa, and Y. Tokura, "Transformation between meron and skyrmion topological spin textures in a chiral magnet," Nature **564**, 95–98 (2018).